

PERFORMANCE OF AN AMBIENT PRESSURE CELL STACK OPERATING UNDER SYNTHETIC GASOLINE REFORMATE

S. Kocha, A. Gaskins, P. Plasse, and D. Wheeler
International Fuel Cells, LLC
South Windsor, CT 06074

KEYWORDS: Fuel Cell, Reformate, PEM

INTRODUCTION

Recently, proton exchange membrane fuel cells (PEMFC) have gained worldwide attention as a possible practical replacement to the internal combustion (IC) engine for automotive applications. International Fuel Cells is actively engaged in PEMFC technology using hydrogen as well as reformed gasoline as a fuel source for automotive and stationary applications. Gasoline reformate from a fuel processor arriving at a PEM cell anode is expected to contain small quantities (10-50 ppm) of carbon monoxide. It is well known that CO is a poison to the platinum anode catalyst when present even in small concentrations of ppm in the fuel feed stream. Carbon monoxide adsorbs on active sites on the surface of the catalyst that would otherwise be available to H₂ for dissociation into monoatomic H_{ads} (Tafel step) for subsequent oxidation. In other words, the Tafel reaction which is the slower of the two step Tafel-Volmer reaction mechanism reaches rate limiting conditions earlier due to unavailability of participating reaction sites. The extensive coverage (~80%) at low (65°C) temperatures causes a precipitous drop in anode limiting current and degradation in cell performance referred to as CO poisoning. There are several ways to deal with the residual CO that enters the fuel cell stack. One is to develop new catalysts that are more tolerant to CO either by the mechanism of CO oxidation using OH⁻ ions at lower potentials. Another is the use of alloys that have components with a lower heat of adsorption to CO. Still a third pathway is to inject small amounts of air into the fuel feed [1,2] so that the CO is oxidized by oxygen at the catalyst surface, thereby recovering surface area for the hydrogen oxidation reaction and raising the cell performance. In the latter case, some hydrogen will also be oxidized, depleting the fuel and, hence, will result in an efficiency loss. A certain amount of heat will also be generated due to the oxidation of both hydrogen and CO.

The reverse shift reaction may also take place, since fuel feed consists of CO₂, which in addition to causing a dilution effect may participate in the production CO or some other reduced form of CO₂ [3]. Thus a poisoning effect due to CO₂ may be observed.

In this paper, we present results on the effect of dilution of fuel, CO, CO₂ poisoning and, its mitigation by air injection, as well as selectivity of air injection.

EXPERIMENTAL

A low loaded (0.10 mg/cm² Pt anode; 0.37 mg/cm² Pt cathode; Gore 15 micron membrane) as well as a higher loaded "CO tolerant" catalyst (0.40Pt-0.20Ru mg/cm² anode; 0.30 mg/cm², 0.40 mg/cm² cathode on Gore 15 micron membrane) were tested with H₂/CO or synthetic reformate gases at the anode while using air on the cathode. The electrochemically active area of the cell was 327 cm². The dry synthetic reformate composition used was CO₂ = 21%, N₂ = 30%, H₂ = 49%. An existing in-house software was used to acquire cell performance data. Special precautions were taken in the experimental test rig to ensure safety in the introduction of air into the fuel stream. Care was taken to ensure that the lower flammable limit (~5% oxygen in hydrogen or ~25% air in hydrogen) was not approached.

Gas chromatographic (GC) mass balance analyses of dry gasses entering and leaving the anode were carried out to determine the CO converted to CO₂ and to better understand the mechanism of CO oxidation particular to this system. GC measurements of dried gases were carried out at the fuel inlet and exit. In these studies CO in pure hydrogen was used rather than synthetic reformate in order to determine both the CO converted as well as CO₂ formed. (The CO₂ formed would not be measurable if synthetic reformate containing 21% CO₂ were used.) Impurities of CO₂ at the inlet, as well as unused oxygen and unoxidized CO (at low air bleeds) at the fuel outlet, were measured. All measurements were repeated 3-4 times for reproducibility.

RESULTS AND DISCUSSION

We report below the data on an MEA in a single cell having 0.1mg/cm² anode platinum loading and 0.37 mg/cm² cathode loading. Results are reported at 65°C and ambient pressure. Hydrogen utilization was 90% and air utilization 30% at 647 mA/cm². Figure 1 shows a "calibration" performance curve using pure H₂, performance curve with 20 ppm CO in H₂, and 0.5% air

injection. The anode polarization loss at 400 mA/cm^2 was $>300 \text{ mV}$. A complete performance curve was obtained at 0.25% air bleed. The air injection reduced the polarization to $\sim 250 \text{ mV}$. At 647 mA/cm^2 , the air injection was increased in discrete steps up to 2.5% at which point the performance loss reached a minimum $\sim 20 \text{ mV}$. Figure 2 shows the discrete steps in which the air bleed was increased at 647 mA/cm^2 . In the last two steps, the CO is shut off after which the air bleed of 2.5% is shut off. A $\sim 5\text{-}10 \text{ mV}$ increase in performance is observed when the CO is turned off.

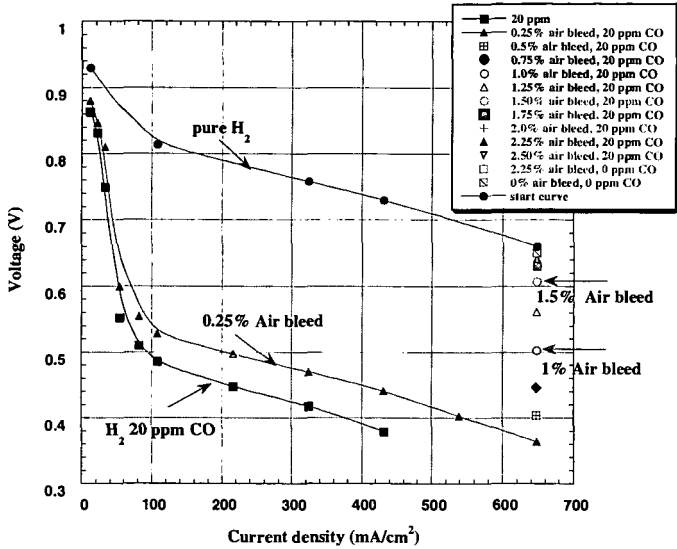


Figure 1 Performance curves depicting the loss in performance with the introduction of 20 ppm CO and the mitigation of CO poisoning with the use of an air bleed in the fuel feed stream. A complete curve with 0.25% air bleed is plotted as well as gain in performance with increasing air bleed at 647 mA/cm^2 at 65°C and 100 kPa .

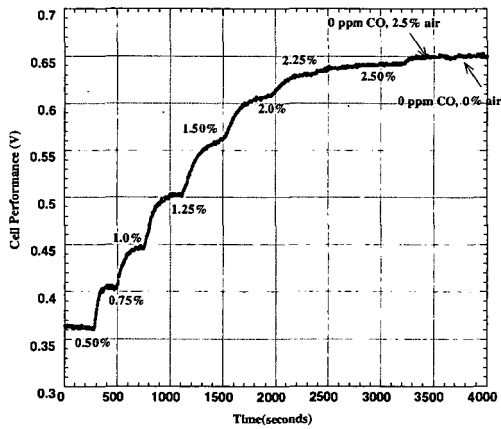


Figure 2 Details of the enhancement in performance during the step wise increase in air bleed at 647 mA/cm^2 of figure 2 at 65°C and 100 kPa .

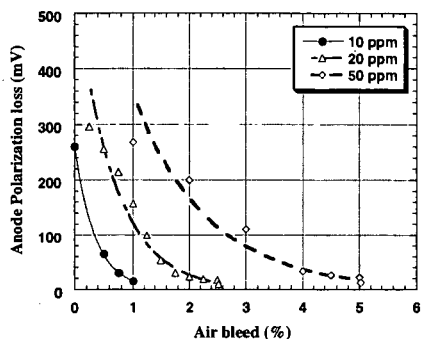


Figure 3 Variation of anode polarization with air bleed as a percentage of total anode fuel flow at 65°C and 100 kPa. (anode platinum loading 0.1 mg/cm²)

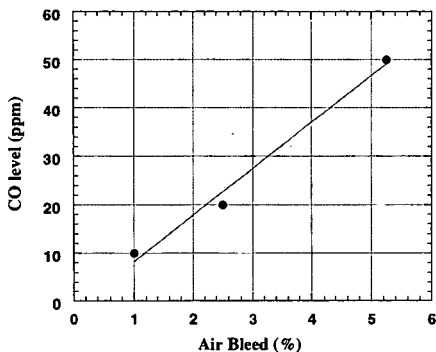


Figure 4 Dependence of the % air bleed required to raise the performance of a CO poisoned MEA (anode platinum loading 0.1 mg/cm²) to within 10-15 mV of its hydrogen-air performance at 65°C and 100 kPa.

The rate at which the performance was enhanced (or anode polarization/cell loss decreased) with increasing % air bleed at 647 mA/cm² is shown in figure 3. The performance loss decreases at an exponential rate with % air bleed. Figure 4 summarizes the approximate amount of %air needed to be injected for different CO amounts in the fuel stream for performance recovery to within ~20 mV. The ratio of air bleed (21% oxygen) to CO level is a constant at about 200 and is a measure of the selectivity of the CO oxidation.

Mass Balance on low loaded (0.10 mg/cm² Pt anode) Pt anode

As described in the experimental section gas chromatographic studies were conducted to determine the mass balance of CO, air, and impurities (CO₂ ~8 ppm) entering and exiting the anode. The air bleed in also contains 0.04% CO₂. The gases measured at the inlet and exit are dry gases. At 20 ppm CO inlet conditions with 2% air injection, the mass balance is shown in table 1. We observed that oxygen in the air bleed is not fully utilized and exits the anode along with CO₂ and even unoxidized CO at low air bleeds. The selectivity of CO oxidation based on the mass balance is of the order of 100:1.

TABLE 1 20ppm CO in hydrogen, 65°C, V_{OC}, 2% air bleed

	<u>Inlet Flow</u>	<u>Exit Flow</u>	<u>Inlet-Exit</u>
CO ppm	20.4	0.0	20.4
CO ₂ ppm	15.0	43.1	28.1
N ₂ %	1.51	1.60	0.10
O ₂ %	0.43	0.11	0.30
CO oxidized	≈20.4ppm		
O ₂ used	≈0.30% = 3000ppm		
O ₂ unused	≈0.11% = 1100ppm		

Figure 5 shows three performance curves, namely the hydrogen-air curve, 50% hydrogen and 50% nitrogen, 49% hydrogen, 30% N₂, and 21% CO₂. (simulated reformat with no CO). The losses due to dilution by N₂ at 647 mA/cm² is ~25 mV and the additional loss due to CO₂ poisoning is ~70 mV. At 647 mA/cm² air was bled into the anode in small increments until the cell performance was recovered. At 0.6% air bleed the performance reaches to within 10-15 mV of the maximum possible diluted performance. Further air bleed did not result in any performance gain. Figure 6 shows the effect of air bleed when the anode is subject to simulated reformat + 10 ppm CO. Combining the results in figures 6 and 7, it appears that the air bleed required for recovering the performance is approximately the sum of that required for CO₂ and CO individually and is ~1.75%.

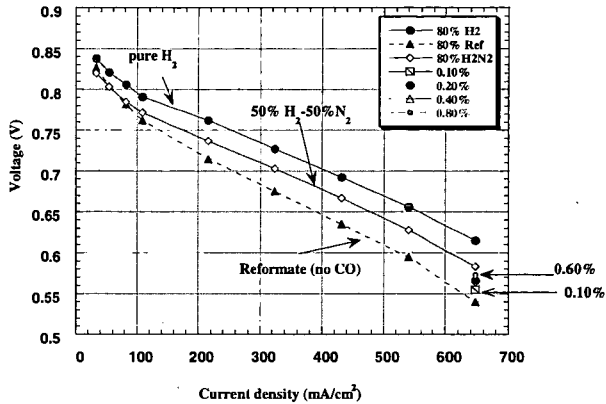


Figure 5 Single Cell Stack Performance with anode gas compositions of pure H₂, H₂-N₂ and simulated reformat containing 49% H₂:21% CO₂:30% N₂ + Air Bleed (% of total anode flow)

High loaded Pt-Ru anodes (0.40Pt-0.20Ru mg/cm²)

Figure 7 compares the effect of reformat with 10 ppm CO with and without air bleed at 538 mA/cm² with time. The air bleed required for this Pt-Ru catalyst with 10 ppm CO in reformat is of the order of 0.6% and less than that for a lower loaded Pt anode (1%) for the same CO ppm in reformat.

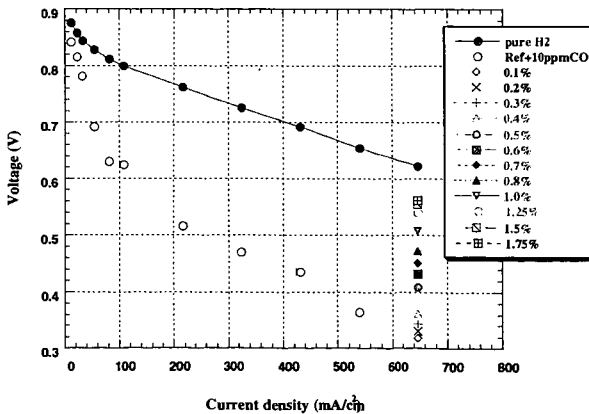


Figure 6 Performance curves showing the effect of reformat containing 10 ppm CO and step increases in air bleed at 647 mA/cm² that recovers the poisoning losses.

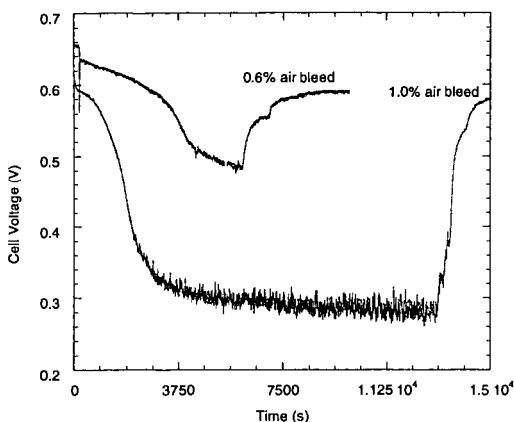


Figure 7 Comparison of cell voltage at constant current density of $647\text{mA}/\text{cm}^2$ versus time. The upper curve corresponds to a Pt-Ru anode of $0.4\text{-}0.2\text{ mg}/\text{cm}^2$ loading and the lower curve corresponds to anode with a Pt loading of $0.3\text{ mg}/\text{cm}^2$. Both cathodes had $0.3\text{ mg}/\text{cm}^2$ of Pt. The PtRu anode shows lower anode polarization losses and a lower air bleed of 0.60% is required to mitigate the poisoning. The cell temperature and pressure are 65°C and 100 kPa .

Voltage Oscillations

In the process of assessing the CO tolerant properties of different anode catalysts by testing for MEA performance, we observe an oscillatory phenomena. At high current densities and/or high CO ppms, the performance of the fuel cell fluctuates systematically with a relatively fixed amplitude and period. Air bled into such an oscillating system causes the oscillations to decline in frequency and eventually dampens out the amplitude. The period of oscillation is quite definite; if air is bled in, the period increases until finally oscillations cease in time when the air bleed is sufficient. With very low anode loadings of $0.1\text{mg}/\text{cm}^2$ oscillations were not observed. Although the total number of available sites is reduced with a lower loading, the fraction of available sites for hydrogen oxidation stays the same following an adsorption isotherm. When the number of available sites are very low, the instrumentation is not sensitive enough to measure low amplitude oscillations.

CONCLUSIONS

The air bleed required to regain the performance and alleviate carbon monoxide poisoning was determined for different CO concentrations in hydrogen. Air injection was also found to recover losses caused by the much milder CO_2 poisoning. The air bleed to recover performance loss due to the combined effect of CO and CO_2 was found to be additive. In the presence of reformat with 10 ppm CO only $\sim 0.5\%$ air bleed was required for a higher ($0.4\text{Pt-}0.2\text{Ru mg}/\text{cm}^2$) loaded Pt-Ru anode. Mass balance of the CO and converted CO_2 as well as excess oxygen were measured using gas chromatography. The amount of air bleed will affect the fuel efficiency of the stack and power plant.

REFERENCES

1. S. Gottesfeld and J. Pafford, *J. Electrochem Soc.*, **1988**, 135, 2651
2. D. Sutton, Report at the **1992 Fuel Cell Seminar**, Tucson, AZ.
3. J. Giner, *Electrochim. Acta*, **1963**, 8, 857

OPTIMAL OPERATING TEMPERATURE AND PRESSURE OF PEM FUEL CELL SYSTEMS IN AUTOMOTIVE APPLICATIONS

Bhaskar Balasubramanian, Frano Barbir and Jay Neutzler
Energy Partners, L.C.
1501 Northpoint Parkway
Suite 102, Technology Center
West Palm Beach, FL 33407

INTRODUCTION

The automotive industry is currently faced with the challenge to develop cleaner and energy efficient vehicles in order to meet the reduced toxic emissions standards. The proton exchange membrane (PEM) fuel cell system offers the most promising solution that would enable both efficiency improvement and emissions reduction in automobiles. Since fuel cells use hydrogen as the fuel, in order to facilitate an early market entry, the stacks are being integrated with reformers (fuel processors) that produce hydrogen from conventional fuels such as gasoline, methanol, natural gas, or propane. It is also a viable technology for decentralized power generation. Gasoline being the established vehicle fuel in terms of supply and distribution is best suited for automotive PEM fuel cell system while natural gas is the popular choice for small residential or stationary power applications.

The PEM fuel cell may be operated at pressures ranging from near ambient to about 6 atm and at temperatures between 50 and 90°C. High power density is obtainable at higher operating pressures but the net system efficiency may be lower on account of the power needed for air compression. High power density is also obtained at the higher operating temperatures, however it may pose a significant challenge for water and heat management especially at lower operating pressure. A lower operating temperature, on the other hand, makes waste heat rejection into the environment difficult particularly in hotter surroundings. Therefore selection of operating temperature and pressure of the automotive PEM fuel cell system must be based on (a) high net system efficiency, (b) small component size, and (c) neutral or positive water balance so that the vehicle does not have to carry on-board water reservoir.

In order to select the optimal operating temperature and pressure of the automotive fuel cell system Energy Partners developed a steady-state mathematical model of the entire fuel cell system that estimates the system and component parameters (such as mass flows, reaction rates, heat fluxes and loads, heat exchanger size, component and net system efficiencies etc.) at various operating temperatures and pressures and at various power levels.

SYSTEM DESCRIPTION

As shown in Figure 1, the automotive fuel cell system consists of the following major components or subsystems:

- Fuel Processor (which includes exhaust heat recovery in burner)
- Compressed Air Delivery
- Fuel Cell Stack
- Heat and Water Management
- Exhaust (Expander)

Figure 2 is a 3-D representation of the complete automotive fuel cell system. The fuel to be reformed in this case is gasoline. Epyx Corp.¹ successfully demonstrated a partial oxidation based fuel processor. Gasoline is reformed to produce a reformat stream consisting of approximately 40% hydrogen, 20% carbon dioxide, and balance nitrogen (dry basis) after CO clean-up. A typical reformat stream leaves the fuel processor at near 160-170°C saturated with water vapor. The wet gas is then conditioned to the stack temperature, the condensed water removed in a separator, and sent to the fuel cell anode fully humidified at that temperature. Compressed ambient air is humidified before it is supplied to the cathode. The unutilized/excess hydrogen from the fuel cell anode exhaust is burnt with the excess air (from the cathode exhaust) in the tail gas catalytic combustor (TGC). Exhaust gases from the TGC are then expanded to recover part of the energy needed for compression. In most applications the fuel cell temperature is controlled using water. However, for an automotive system like the one described here, an anti-freeze liquid such as propylene glycol is preferable. Heat from the coolant loop is rejected in an air-cooled heat exchanger or radiator. Water is consumed in the fuel processor in the steam-reforming and shift reactions, and in the humidification of air. In addition water is needed as the cooling medium in the fuel processor. Water is produced in the stack as a result of the reaction between H₂ and O₂, and also in the TGC by combusting hydrogen. For an automotive system it is important to have a neutral water balance to avoid on-board de-ionized water supply. Therefore, liquid water is separated from all gas streams (fuel cell exhaust gases and the TGC exhaust) and conditions maintained so as to achieve neutral water balance. The electrical power generated by the fuel cell is used to power the auxiliary

oxidation. Thus based on the amount of hydrogen required, the model calculates the mass flows of the reacting species.

Fuel Cell:

The stoichiometric amounts of H₂ and O₂ consumed in the electrochemical reaction in the fuel cell are computed by Faraday's law. However, since neither H₂ nor O₂ is present as pure gas excess amounts are supplied to the fuel cell and the unused H₂ is burnt with the unused O₂ in the TGC later for heat integration with the reformer. The H₂ stoichiometric ratio depends on the actual fuel cell flow field design. The power generated by the fuel cell stack is a product of the individual cell voltage, current density and the number of cells. The current and voltage are related according to the polarization curve and an experimentally determined curve is used in the model. The fuel cell efficiency is defined as the ratio of the electrical power output to the heating value of H₂ fed.

$$\eta_{FC} = (I \cdot V_{cell}) / (\Delta H_{H_2} \cdot \text{Mass H}_2 \text{ fed})$$

It can thus be seen that high efficiency is obtainable at higher fuel cell potential and lower H₂ stoichiometry. However for any given power output a high fuel cell operating voltage leads to larger stack.

Air Supply and Exhaust Heat Recovery:

Unused H₂ from the fuel cell is combusted in the TGC and the heat generated is utilized in the fuel processor for preheat and/or steam generation. Combustion being exothermic, temperature of the exhaust gases is relatively very high and the heat is utilized in an expander to generate part of the power needed for air compression. It will be explained later that an expander is necessary for a pressurized system. Power recovered in the expander is computed using isentropic equations. Similarly, based on O₂ flow needed for the fuel cell, air flow is computed and compressor is sized accordingly.

Water and Heat Management:

The coolant flow is computed depending upon the heat generated in the fuel cell and the operating temperature. Accordingly, the model calculates the cooling duty needed in the coolant loop and estimates size and other parameters for the radiator.

System Efficiency:

The overall system efficiency is a product of the efficiencies of the fuel processor, the PROX unit, the fuel cell and balance of plant (η_{BOP}). η_{BOP} is the ratio of the net power to the gross power produced by the fuel cell. The difference between gross power and net power includes power needed to run compressor/expander, fans, pumps, solenoid valves, relays, controller, etc.

RESULTS AND DISCUSSION

The model briefly described above was used to perform steady state simulations to calculate the following system parameters (based on the input parameters and assumptions outlined in Table 1): (a) fuel consumption, air and water requirements; (b) fuel cell parameters (size and number of cells); (c) parasitic load requirements or BOP analysis.

Table 1. Input parameters

Net power output:	50 kW
Fuel cell polarization curve:	EP laboratory results
Cell nominal voltage:	Variable
Operating pressure:	Variable from 101.3 to 308 kPa
Operating temperature:	Variable from 50 to 80 °C
Reactants humidification:	both gases 100% RH at operating temp.
Stack ΔT :	10°C
Stack pressure drop:	15 and 30 kPa
Stoichiometry:	2.0 cathode; 1.17 anode
Compressor efficiency:	0.8
Expander efficiency:	0.8
Expander inlet temperature (max):	150°C
Reformer efficiency:	0.8 (LHV)
Reformer fuel equivalence ratio:	3.13
Water/fuel ratio in reformer (mol):	22.84
Fuel:	Octane (C ₈ H ₁₈)
PROX stoichiometry:	2 (efficiency 0.97)
Reformer pressure drop:	15 and 30 kPa
Ambient conditions:	101.3 kPa, 30°C, 60%RH

Figure 3 shows the dependence of the system efficiency on fuel cell operating temperature and pressure. For the pressurized system a higher operating temperature results in a somewhat higher system efficiency and vice-versa for a low temperature system, which is mainly due to: (a) at low operating pressure, the expander recovers very less or no power, and (b) high operating temperature when coupled with low pressure necessitates large amounts of water recovery in the condenser which results in a very high parasitic load for the condenser fan. It should be noted that in these comparisons, the fuel cell voltage at nominal power was kept constant at 0.7 V/cell. A higher cell voltage results in higher efficiency but results in less power density (W/cm^2) or in other words a larger stack. Figure 4 shows relative stack sizes as a function of temperature and pressure at constant nominal system efficiency. High temperature and high pressure lead to the smallest stack size.

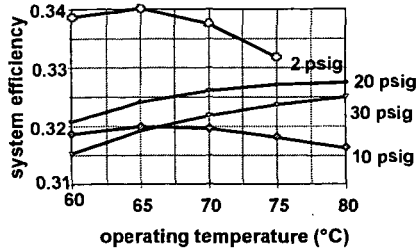


Figure 3. Effect of Operating Temperature and Pressure on System Efficiency

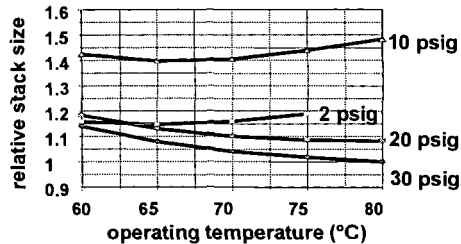


Figure 4. Effect of Operating Temperature and Pressure on Stack Size

However stack size is not the only criteria in selecting operating temperature and pressure. Size and performance of other components such as the fuel processor and radiator are also affected by pressure and temperature. Figure 5 shows the variation in heat load on the condenser and radiator with operating temperature and pressure. High temperature when coupled with low pressure shifts the heat load from the condenser to the radiator. On the other hand, high pressure and low temperature results in maximum heat rejection in the radiator. The major difference between these two components is that the radiator is liquid-to-gas heat exchanger while the condenser is a gas-to-gas heat exchanger. Heat transfer coefficients are significantly lower for the condenser, which means that for a given heat load the condenser requires much larger heat transfer area than the radiator. Figure 6 compares the heat transfer areas for the condenser and radiator as a function of temperature and pressure. The calculations assume a liquid/gas heat transfer coefficient of $60 W/m^2/^\circ C$ and gas/gas coefficient of $15 W/m^2/^\circ C$ and a fin-to-tube area of 10. The system that operates at high pressure (30 psig) and low temperature ($60^\circ C$) requires the smallest heat exchanger. For automotive fuel cell systems heat exchanger size may very well be a limiting factor. At 30 psig and $60^\circ C$, there is no need for a condenser since all heat is rejected in the radiator.

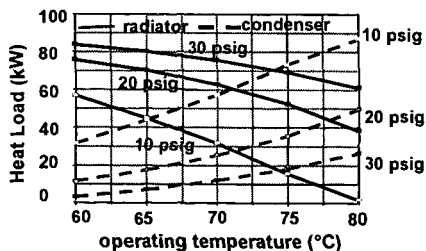


Figure 5. Radiator and Condenser Heat Load (50 kW net, constant efficiency)

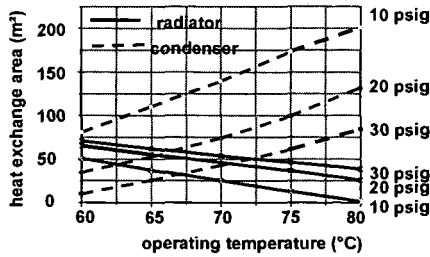


Figure 6. Required Heat Exchanger Area for a 50 kW (net) System

In all cases neutral water balance was accomplished such that enough water was condensed in the system to make up for the reformer process water and for air humidification. Water management poses a concern in systems that operate at low pressures and high temperatures since large amounts of water are needed for humidification.

With certain assumptions and limitations, the model also simulates the performance at off-design conditions such as partial loads and ambient conditions. Figure 7 shows projected system efficiency at various power levels. At 25% net peak power, the net system efficiency is around 39%. However for a realistic case, since the efficiencies of the compressor and expander are lower at lower pressures and lower power levels, the system efficiency is around 37%. Again, higher efficiencies (>40%) are obtainable at higher cell voltages at peak power. Ahluwalia et. al.² have shown that 44.8% system efficiency is obtainable at 0.8 V/cell and 90% hydrogen utilization.

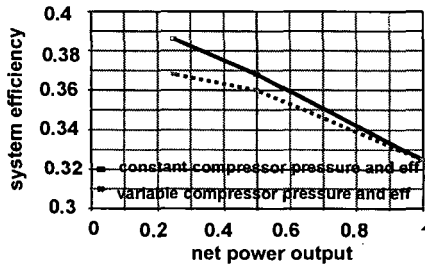


Figure 7. System Efficiency as Function of Net Power Output (30 psig, 80°C, 50 kW - peak power)

CONCLUSIONS

The numerical steady state model developed for performance simulation of the PEM fuel cell automotive system has proven to be a valuable tool for component sizing, trade-off analysis by varying system configurations, and optimizing system pressure and temperature. Results suggest that an automotive system should operate at high pressure (30 psig), but an expander must be used to recover power used for compression. Surprisingly, results indicate that a low temperature (60°C) results in smallest size of heat exchanger if neutral water balance is mandated. The model also predicts system efficiency at different loads. Higher efficiencies may be achieved at higher cell voltages, but that would result in large fuel cell stack, which may be a limiting factor for automotive applications with the state-of-the-art fuel cells.

ACKNOWLEDGEMENT

This work was supported by the U.S. Department of Energy, Office of Advanced Automotive Technologies, under contract no. DE-FC02-97EE50476.

REFERENCES

1. W.L. Mitchell, "Integrated Power System for Transportation - Advanced Fuel Processor Development", Fuel Cells for Transportation 98, Contractors Annual Progress Report, Vol. 1, pp23-27, U.S. Department of Energy, OAAAT, Washington D.C., November 1998.
2. R.K. Ahluwalia, E.D. Doss, H.K. Geyer and R. Kumar, "Pressurized POX-Reformed Gasoline PEFC System", presented at the Pressure Effects Workshop, Argonne National Laboratory, Argonne, IL, December 1998.

PREPARATION OF Pt-Ru OR Pt-Mo SUPPORTED CATALYSTS FOR PEM OR DIRECT METHANOL FUEL CELLS FROM SINGLE-SOURCE MOLECULAR PRECURSORS

C. M. Lukehart¹, D. L. Boxall¹, J. D. Corn¹, M. Hariharasarma¹, W. D. King¹, K. C. Kwiatkowski¹, E. S. Steigerwalt¹, and E. A. Kenik²

(1) Department of Chemistry, Vanderbilt University, Nashville, TN 37235

(2) Metals and Ceramic Division, Oak Ridge National Laboratory, Oak Ridge, TN 37831

KEYWORDS: Binary alloy catalysts; PEM fuel cell catalysts; Direct methanol fuel cell catalysts

ABSTRACT

An overview of the synthesis and characterization of several Pt-Ru or Pt-Mo/Vulcan carbon nanocomposites and one Pt-Ru/graphitic carbon nanofiber nanocomposite is provided. Each binary metal alloy nanocluster composition is accessed through the thermal decomposition of a single-source molecular precursor containing the desired metal stoichiometry. Microwave heating techniques are used to form a Pt-Ru/Vulcan carbon nanocomposite within one minute of thermal treatment. The metal stoichiometry of individual alloy nanoparticles has been determined from on-particle EDS measurements obtained using HR-TEM(FEG) instrumentation. Preliminary DMFC testing results are also summarized.

INTRODUCTION

There is currently much interest in developing metal alloy catalysts having improved reactivity as anode catalysts in fuel cells.¹ Specifically, Pt-Ru alloys are commonly used as anode catalysts in direct methanol fuel cells (DMFCs) for the electrocatalytic oxidation of methanol.² Pt-Mo catalysts are of interest as anode catalysts in PEM fuel cells operating on reformato fuels due to their higher CO-tolerance relative to platinum metal catalysts.³ Even though fuel cell anode catalysts might undergo significant chemical changes during conditioning or aging within a working fuel cell environment, there is a need to determine the dependence of fuel cell catalytic activity on the precise metal alloy stoichiometry of the initial catalyst as prepared. For practical considerations, there is interest in preparing fuel cell anode catalysts on conducting carbon supports to minimize the amount of noble metal required in a working fuel cell.

We are investigating the use of single-source molecular precursors as a means to better control the elemental stoichiometry of individual metal alloy nanoparticles formed on conducting carbon supports. While others have used heteronuclear clusters to prepare ruthenium-rich Pt-Ru/carbon nanocomposites of low total metal weight percent,⁴ we have used heteronuclear noncluster or cluster compounds to prepare several Pt-Ru or Pt-Mo/carbon nanocomposites having high total metal loading and a platinum atomic percent of 50% or greater. In this report, we provide (1) an overview of the synthesis and characterization of several Pt-Ru or Pt-Mo/Vulcan carbon nanocomposites, (2) the rapid synthesis of a Pt,Ru/Vulcan carbon nanocomposite using microwave heating, (3) the synthesis of a Pt,Ru/graphitic carbon nanofiber (GNF) nanocomposite, (4) the determination of the metal alloy stoichiometry of individual alloy nanoclusters, and, (5) preliminary results from testing selected Pt-Ru/Vulcan carbon nanocomposites as DMFC anode catalysts.

EXPERIMENTAL

The single-source molecular precursors $[(\eta^3\text{-}\eta^3\text{-2,7-dimethyloctadienediy})\text{RuCl}(\mu\text{-Cl})_2\text{PtCl}]_n$, **1** (L= PPh₃, PEt₃, or ethylene),⁵ $[\text{Cl}_2\text{Pt}(\mu\text{-bipyrimidine})\text{Ru}(2,2'\text{-bipyridine})_2][\text{X}]_n$, **2** (X= BF₄ or PF₆),⁶ $[\text{Pt}_3(\text{PPh}_2\text{CH}_2\text{PPh}_2)_3\{\text{HgRu}(\eta\text{-C}_5\text{H}_5)(\text{CO})_2\}_2][\text{PF}_6]_2$, **3**,⁷ $[\text{Ru}\{\mu\text{-2,3-bis}(2\text{-pyridyl})\text{-quinoxaline}(\text{PtCl}_2)_3[\text{BF}_4]_2$, **4**,⁸ $[\text{Pt}(\text{pyridine})_2][\text{Mo}(\eta\text{-C}_5\text{H}_5)(\text{CO})_3]_2$, **5**,⁹ $[\text{Pt}(1,5\text{-cyclo-octadiene})(\text{Me})][\text{Mo}(\eta\text{-C}_5\text{H}_5)(\text{CO})_3]$, **6**,¹⁰ $[\text{Pt}(\text{PPh}_2\text{CH}_2\text{PPh}_2)_3\text{Mo}(\eta\text{-C}_5\text{H}_5)(\text{CO})][\text{BPh}_4]$, **7**,¹¹ where prepared by literature procedures, modifications of literature procedures, or by novel methods. Carbon supports included VulcanTM Carbon XC-72R (Cabot Corporation) or GNFS prepared using published procedures.¹²

Metal alloy/carbon nanocomposites were prepared by depositing single-source molecular precursors from a solution onto the appropriate carbon support through evaporation of the solvent. Multiple depositions were sometimes employed. Thermal degradation of the deposited molecular precursors typically occurred in reactive [air (up to 350°C) and/or getter gas (350-650°C)] or inert [nitrogen (650-700°C)] gaseous environments. Thermal treatments were conducted either in a tube furnace using gas flow rates typically of 150 mL/min and heating rates typically of 15°C/min or in a microwave oven (Sharp Corporation, Model R-2M52B) operating at 2.45 GHz with a fixed power level of 600 Watts. Samples prepared by microwave heating were contained in a vial surrounded by a thermal bath of Vulcan carbon. Chemical microanalysis was performed by Galbraith Laboratories, Knoxville, TN.

Low-resolution TEM micrographs were obtained using a Philips CM20T transmission electron microscope operating at 200 kV and equipped with an EDAX detector, while HR-TEM micrographs and on-particle EDS spectra were obtained at ORNL using a Philips CM200FEG

TEM operating at 200 kV and equipped with an Oxford light element EDS detector and an EMI SPECT Vision data acquisition system. Powder XRD scans were obtained on a Scintag X1 diffraction system.

RESULTS

As shown in Table I, complexes 1 ($L=C_2H_4$), 2 ($X=BF_4$), 3, and 4 which have Pt/Ru metal stoichiometries of 1:1, 1:1, 3:2, and 3:1, respectively, serve as single-source molecular precursors for Pt-Ru/Vulcan carbon nanocomposites having metal alloy fcc lattice constants consistent with those observed for bulk Pt-Ru alloys containing the same respective Pt/Ru metal ratios. These nanocomposites have metal loadings of 25-39 weight percent and metal alloy nanoparticle average diameters of 2.7-7.5 nm (as volume-weighted average diameters determined from XRD peak widths) or 2.6-5.7 nm (as number-averaged diameters determined from TEM micrographs). Only monomodal histograms of metal alloy particle sizes are observed.

Table I. Analysis of Selected Pt-Ru/Vulcan Carbon Nanocomposites

Metal Alloy Composition	Molecular Precursor	Total M wt. %	Ave. Dia. (nm) (XRD/TEM)	fcc a_{obs} (Å)	fcc $a_{expected}$ (Å)
Pt ₁ Ru ₁	1 ($L=C_2H_4$)	39	2.7/2.6	3.858(6)	3.864
Pt ₁ Ru ₁	2 ($X=BF_4$)	33	4.2/4.3	3.86(1)	3.864
Pt ₃ Ru ₂	3	25	7.5/3.9	3.875(2)	3.876
Pt ₃ Ru ₁	4	37	6.7/5.7	3.911(1)	3.895

As shown in Table II, complexes 5, 6, and 7 which have Pt/Mo metal stoichiometries of 1:2, 1:1, and 3:1, respectively, serve as single-source molecular precursors for Pt-Mo/Vulcan carbon nanocomposites having bulk metal analyses consistent with the Pt-Mo content of the respective molecular precursor. The value of the fcc lattice constants observed for these alloy nanocomposites is not a reliable indicator of Pt/Mo composition due to the very similar atomic radii of Pt and Mo. Full-profile Rietveld refinement of the powder XRD scans of these pure nanocomposites reveals best convergence at Pt/Mo ratios near to the metal content of the molecular precursors. These nanocomposites have metal loadings of 43-58 weight percent and metal alloy nanoparticle average diameters of 3.9-12.2 nm (as determined from XRD peak widths) or ca. 3.5 nm (as determined from TEM micrographs). Only monomodal histograms of metal alloy particle sizes are observed.

Table II. Analysis of Selected Pt-Mo/Vulcan Carbon Nanocomposites

Metal Alloy Composition	Molecular Precursor	Total M wt. %	Ave. Dia. (nm) (XRD/TEM)	fcc a_{obs} (Å)	Pt:Mo Ratio by ICP-OES
Pt ₁ Mo ₂	5	58	12.2/3.5	3.9144(1)	0.5
Pt ₁ Mo ₁	6	52	3.9/...	3.9183(1)	0.9
Pt ₃ Mo ₁	7	43	4.6/3.4	3.9124(1)	2.9

Deposition of molecular precursor 1 ($L=C_2H_4$) having a Pt:Ru stoichiometry of 1:1 onto Vulcan carbon followed by microwave irradiation under appropriate gaseous atmospheres over a total heating period of less than 60 seconds gives the expected Pt₁Ru₁/carbon nanocomposite. A TEM micrograph of one such nanocomposite is shown in Figure 1. HR TEM micrographs reveal lattice fringes on the Pt₁Ru₁ particles consistent with a 1:1 alloy composition. A histogram of PtRu nanoparticle diameters reveals an average nanocluster diameter of 3.2 nm with a standard deviation of 0.66 nm and a size distribution of only ca. 1.4 nm at full-width-at-half-height. The Pt₁Ru₁ nanoclusters give a diffraction pattern consistent with a fcc cell exhibiting broad peaks as expected from the small average particle size of the Pt₁Ru₁ nanoclusters. Peak positions give a fcc lattice parameter of 3.867 Å, as expected for a 1:1 Pt:Ru alloy (see Table I).

Pt₁Ru₁ nanoclusters can also be formed on GNF carbon supports using complex 1 ($L=C_2H_4$) as a single-source molecular precursor. Deposition of this precursor onto a GNF support followed by the appropriate thermal treatment gives a Pt₁Ru₁/GNF nanocomposite, as shown in Figure 2. The metal alloy nanocrystals are highly dispersed on the GNF support.

The on-particle Pt:Ru metal stoichiometry of several Pt-Ru/Vulcan carbon nanocomposites prepared from single-source molecular precursors has been determined by EDS measurements using HR-TEM(FEG) microscopy. Pt:Ru atomic ratios obtained as raw data were corrected for an apparent loss of Ru from the outermost layer of the individual particles. A plot of these corrected Pt:Ru atomic ratios for a number of individual alloy particles of one such sample is shown in Figure 3. The major contribution to the experimental uncertainties shown is the error associated with the counting statistics of the detector.



Figure 1. TEM micrograph of a Pt₁Ru₁/Vulcan carbon nanocomposite prepared by microwave heating.



Figure 2. TEM image of a Pt₁Ru₁/GNF nanocomposite prepared using **1** ($L-C_2H_4$) as a single-source precursor for the alloy nanoclusters.

Such on-particle EDS measurements typically indicate that the Pt:Ru atomic ratio of individual metal alloy particles fall within one or two standard deviations of the bulk Pt:Ru elemental stoichiometry. As shown in Table III, the calculated weighted average of Pt:Ru atomic ratios determined from individual alloy nanoclusters within four different alloy/Vulcan carbon nanocomposites fall close in value to the bulk alloy stoichiometry as determined by chemical microanalysis. The experimental uncertainty of alloy compositions determined by chemical microanalysis has not been determined.

Selected Pt-Ru/Vulcan carbon nanocomposites prepared using complexes of type **1** or **2** as single-source molecular precursors have been tested as anode catalysts in DMFCs. Details of these testing procedures will be presented elsewhere. One such Pt₁Ru₁/Vulcan carbon nanocomposite exhibited a higher activity for methanol oxidation at open circuit and at low current densities than did a comparable commercial catalyst, while another Pt₁Ru₁/Vulcan carbon nanocomposite outperformed a comparable commercial catalyst at all higher current densities.

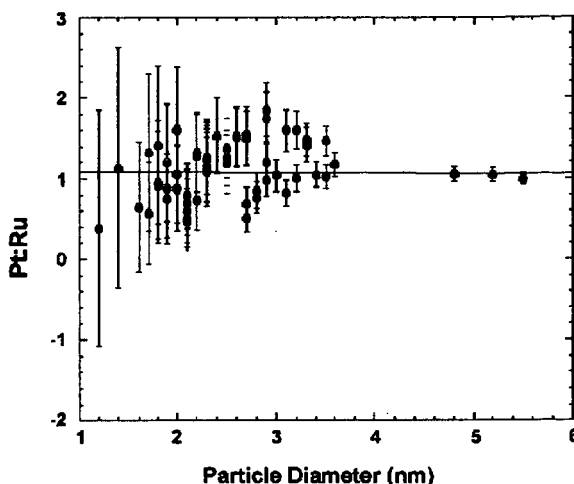


Figure 3. Corrected Pt:Ru atomic ratios for individual metal alloy nanoparticles as a function of nanoparticle size.

Table III. Comparison of Pt:Ru Atomic Ratios Determined by Chemical Analysis and by On-Particle EDS Analysis

<i>Alloy/Vulcan C. Nanocomposite</i>	D_{TEM} (nm)	D_{EDS} (nm)	<i>Chemical Analysis (Pt,Ru₁)</i>	<i>Average EDS (Pt,Ru₁)</i>
Pt ₁ Ru ₁	3.4 (0.9)	2.6 (0.8)	1.08	1.11 (0.03)
Pt ₁ Ru ₁	----	2.4 (0.4)	----	1.00 (0.06)
Pt ₁ Ru ₁	2.6 (0.9)	3.0 (0.8)	0.90	0.88 (0.04)
Pt ₁ Ru ₁	5.7 (3.1)	3.2 (0.7)	3.20	2.83 (0.11)

DISCUSSION

Seven heteronuclear noncluster or cluster complexes have been successfully used as single-source molecular precursors for the preparation of Pt-Ru or Pt-Mo/Vulcan carbon nanocomposites in which the metal stoichiometry of the molecular precursor provides significant control over the metal content of the resulting binary metal alloy nanoclusters. Thermogravimetric analysis of the thermal decomposition of the heptanuclear precursor **3** reveals a single mass-loss event corresponding to loss of the mercury content of the precursor. This result indicates that volatile main group metals can serve as bridging atoms in cluster precursors without being incorporated stoichiometrically into the resulting alloy nanocluster. In addition, this synthetic strategy can be used to prepare metal alloy/Vulcan carbon nanocomposites having high metal loading while maintaining relatively small average particle sizes for the alloy phase. Independent determination of the metal stoichiometry of metal alloy nanoclusters using full-profile Rietveld analysis of XRD patterns is possible and is typically reliable to within a 5 weight % variation of the content for each metal.

Pt₁Ru₁/Vulcan carbon nanocomposites can be prepared very rapidly (<1 min) from deposited single-source molecular precursors using microwave heating of the conductive, particulate support. Normal thermal processing of deposited precursors to give binary metal alloy/Vulcan carbon nanocomposites using tube furnace heating requires typically 2-4 hours of thermal treatment. In addition to the rapid formation of the nanocomposite, microwave heating apparently minimizes metal diffusion on the carbon support to afford metal alloy nanoclusters having more narrow particle size distributions. The general scope of this synthetic method is being investigated.

The successful formation of Pt₁Ru₁/GNF nanocomposites using a single-source molecular precursor is a unique method for obtaining metal alloy nanoclusters on a support having defined structural variety. GNFs can be prepared in which the graphite planes are oriented parallel, perpendicular, or in a herringbone pattern relative to the long axis of the carbon nanofiber. Growth of metal alloy nanoclusters on such ordered carbon supports provides an opportunity to study metal nanocluster-carbon matrix effects and DMFC activity as a function of the atomic and electronic structure of the carbon support. Such studies are under active investigation.

A critical factor in evaluating the practicality of preparing metal alloy nanoclusters by any synthetic method is the direct determination of the metal stoichiometry of individual alloy nanoparticles. By using HR-TEM(FEG) techniques, the metal stoichiometry of individual Pt-Ru alloy nanoclusters has been determined. Preliminary data indicate that metal alloy nanocluster composition is controlled to a high degree by the metal stoichiometry of the single-source precursor used in the synthesis. Further study of truly on-particle metal analysis will explore the general validity of this synthetic method. The observation of a partial loss of Ru during these on-particle analyses was unexpected. Interestingly, the extent of this Ru loss is dependent on alloy particle size and can usually be corrected for by assuming Ru loss from only the outermost unit cell thickness of the metal nanocluster. Due to the known volatility of ruthenium oxides, these results are consistent with the known presence of oxidized Ru species on the surfaces of Pt-Ru nanoparticles.¹³ More detailed confirmation of this observation is anticipated. On-particle analysis of the metal alloy stoichiometry of the Pt-Mo/Vulcan carbon nanocomposites mentioned above (as well as others) is also under investigation.

CONCLUSIONS

Metal alloy/carbon nanocomposites can be formed using single-source molecular precursors to provide considerable control of the metal stoichiometry of the resulting binary metal nanocluster phase. Rapid thermal treatment using microwave heating affords metal alloy/carbon nanocomposites in which the metal nanoclusters have relatively narrow particle size distributions. True on-particle metal stoichiometries can be measured using HR-TEM(FEG) techniques; however, a correction for metal loss possibly due to the presence of surface oxidized species might be necessary for very small alloy particles. Study of the general scope of using this synthetic strategy to prepare binary, ternary, or higher order metal alloys is underway.

ACKNOWLEDGMENTS

Research support provided by the U.S. Army Research Office under grant numbers DAAH04-95-1-0146, DAAH04-96-1-0179, DAAH04-96-1-0302 and DAAG55-98-1-0362 is gratefully acknowledged by C.M.L. On-particle EDS and HR-TEM measurements performed at Oak Ridge National Laboratory were supported by the Shared Research Equipment (SHaRE) User Facilities at ORNL under contract DE-AC05-76OR00033 and by the U.S. Department of Energy under contract DEAC0596OR22464 with the Lockheed Martin Energy Research Corporation.

REFERENCES

- (1) Hamnett, A. *Catal. Today* **1997**, *38*, 445.
- (2) Reddington, E.; Sapienza, A.; Gurau, B.; Viswanathan, R.; Sarangapani, S.; Smotkin, E. S.; Mallouk, T. E. *Science* **1998**, *280*, (5370), 1735.
- (3) Grgur, B.; Zhuang, G.; Markovic, N.; Ross, P. N. *J. Phys. Chem. B* **1997**, *101*, 3910.
- (4) (a) Nashner, M. S.; Frenkel, A. I.; Somerville, D.; Hills, C. W.; Shapley, J. R.; Nuzzo, R. G. *J. Am. Chem. Soc.* **1998**, *120*, 8093. (b) Hills, C. W.; Nashner, M. S.; Frenkel, A. I.; Shapley, J. R.; Nuzzo, R. G. *Langmuir* **1999**, *15*, 690.
- (5) Severin, K.; Polburn, K.; Beck, W. *Inorg. Chim. Acta* **1995**, *240*, 339.
- (6) Sahai, R.; Rillema, D. P. *Inorg. Chim. Acta* **1986**, *118*, L35.
- (7) King, W. D.; Lukehart, C. M. *J. Cluster Sci.* **1998**, *9*, 107.
- (8) Rillema, D. P.; Sahai, R. *J. Chem. Soc., Chem. Commun.* **1986**, 1133.
- (9) Braunstein, P.; Dehand, J. *J. Organometal. Chem.* **1970**, *24*, 497.
- (10) Fukuoka, A.; Sadashima, T.; Endo, I.; Ohashi, N.; Kambara, Y.; Sugiura, T.; Miki, K.; Kasai, N.; Komiya, S. *Organometallics* **1994**, *13*, 4033.
- (11) Ferguson, G.; Lloyd, B.; Puddephatt, R. J. *Organometallics* **1986**, *5*, 344.
- (12) Nemes, T.; Chambers, A.; Baker, R. T. K. *J. Phys. Chem. B* **1998**, *102*, 6323.
- (13) Rolison, D. R.; Hagans, P. L.; Swider, K. E.; Long, J. W. *Langmuir* **1999**, *15*, 774.

SELECTIVE CATALYTIC OXIDATION OF CO IN H₂ FOR FUEL CELL APPLICATIONS

Olga Korotkikh and Robert Farrauto
Engelhard Corporation
101 Wood Avenue
Iselin, New Jersey 08830-0770

KEYWORDS: selective oxidation of CO; PEM fuel cells; monoliths

ABSTRACT

A critical issue for the PEM fuel cell is the ability to delivery clean H₂ to the anode electrode the kinetics of which are greatly hindered by traces of CO present from the hydrocarbon steam reforming and water gas shift processes. A technology receiving much attention is the selective oxidation of CO to CO₂. Ideally the catalyst must selectively oxidize about 1% (10,000 ppm) CO to less than 5 ppm without oxidizing any of the 30-70% H₂ present.

This paper will describe performance results of a newly developed catalyst for selective oxidation of CO for PEM fuel cell applications. The effect of space velocity, concentrations of CO, O₂/CO ratios and temperature on activity and selectivity will be presented.

INTRODUCTION

Development of the proton exchange membrane (PEM) fuel cell has been considerable during the last 10 years advancing the commercial possibilities for generating clean and efficient power for stationary and mobile source applications (1, 2). The system operates at about 70-80°C using H₂ as the anode fuel. Given the extensive infrastructure existing for natural gas (stationary source applications) and gasoline (mobile source) these are the preferred sources of H₂. The production of clean H₂ for the chemical industry from hydrocarbon feeds (3) is accomplished by a series of catalytic steps including desulfurization, steam reforming, water gas shift and CO removal by either selective oxidation, methanation or pressure swing absorption. All of these technologies are now being reviewed for possible use in the fuel cell.

In the early 1960's Engelhard developed and commercialized the Selectoxo™ catalyst and process for H₂ plants (4-6). The heart of this technology is a highly selective catalyst, which oxidizes up to 10,000 ppm CO without significantly oxidizing the 70% H₂ (dry) present. CO levels were reduced to less than 5 ppm under steady state conditions (50°C, 10,000 h⁻¹ and 200-400 psig). The Selectoxo™ system was located downstream from the CO₂ and H₂O scrubber. For fuel cell applications the catalyst must operate at much higher space velocities at temperatures above about 90°C at ambient pressure in the presence of large amounts of CO₂ and H₂O. Furthermore, it must be designed for transient operation since power demands will vary considerably depending on the application. A large consumption of H₂ is undesirable since it decreases power generation and complicates heat management. Therefore, having a catalyst with high selectivity is critical.

EXPERIMENTAL

The Selectoxo™ catalyst contains 0.5% Pt supported on γ -alumina 1/8 inch tablets promoted with a base metal oxide. The alumina is impregnated with salts of Pt and base metal oxide, dried and calcined. The composition of the new catalyst has been modified and prepared as a powder suitable for deposition onto a monolith structure. We call this material monosel. The cordierite monolith is 400 cells per square inch and is dipped into a water slurry of the catalyst, dried and calcined. Typically washcoat loading of about 1.5 g/in³ were obtained. For direct testing of powdered catalysts they were pressed and crushed into particles 40-60 microns in size.

The test gas contained between 1000 and 5000 ppm CO, 20 % H₂, 10% H₂O and varying O₂ to CO ratios with the balance N₂. When powders were tested they were diluted in a 1:2 ratio of catalyst to quartz. Monoliths were wrapped with insulation and fitted into the 1 inch ID quartz reactor. A control thermocouple was positioned in the inlet section of the catalyst bed.

The consumption of CO and generation of CO₂ was measured with a California Analytical Instruments infrared gas analyzer. O₂ consumed was measured with a Rosemount electrochemical analyzer. The generation of hydrocarbons was monitored with a Rosemount Analytical flame ionization analyzer, but under the conditions of these experiments here none was ever detected.

RESULTS

The comparison of powdered Pt/Al₂O₃ with monosel, at equal concentrations of Pt, at 90 and 150°C and O₂/CO ratios of 0.5 and 0.75 are shown in Table 1. The powder volumetric space velocity (VHSV) is 120,000 h⁻¹. The presence of the promoter metal oxide in monosel significantly increases the CO activity and conversion (X_{CO}) while maintaining excellent selectivity of O₂ for CO (X_{O₂} for CO). Under all conditions the Pt/Al₂O₃ never obtains high CO conversions relative to monosel under realistic operating temperatures up to 150°C.

Figures 1 and 2 demonstrate the influence of oxygen excess above stoichiometric at different temperatures and space velocities for monosel deposited on a monolith. At 90°C and a VHSV of 20,000 hr⁻¹ increasing oxygen improves the activity of the catalyst, but the selectivity decreases. At O₂/CO = 1 conversion of CO reaches 100% with the O₂ selectivity for CO about 50% (Figure 1).

Raising the temperature to 150°C (Figure 2) at a monolith VHSV of 80,000 hr⁻¹ gives almost 100% CO and O₂ conversions at O₂/CO = 1.5. The O₂ selectivity for CO is 33%.

The results for 2000 and 5000 ppm CO are presented in the Table 2. At 90°C increasing the CO concentration from 2000 to 5000 ppm, under stoichiometric conditions (O₂/CO = 0.5), shows a constant CO conversion of 69%. The selectivity of O₂ for CO improves from 66 to 77.6%. Increasing the O₂/CO ratio to 0.75 increases CO conversion to almost 97% with similar selectivities of 64 vs. 68%. At O₂/CO = 1.0 the CO conversion reaches 100% while the selectivity decreases to about 50%. At 150°C 100 % conversion of CO is achieved at both 2000 and 5000 ppm at an O₂/CO = 1 with selectivities of about 50%. As the O₂/CO conversion is decreased from 0.75 to 0.5 the CO conversion decreases, but the total O₂ conversion remains almost 100% with an O₂ selectivity for CO of about 58% for 2000 ppm and 65% at 5000 ppm.

CONCLUSIONS

1. At 90°C, VHSV = 20,000 hr⁻¹ and O₂/CO = 1 conversion of CO is about 100% with the O₂ selectivity for CO about 50%.
2. At 150°C, VHSV = 80,000 hr⁻¹ and O₂/CO = 1.5 conversion of CO is about 100% with the O₂ selectivity for CO about 33%.
3. CO conversions of 100 % are achievable at O₂/CO = 0.75 (at 5000 ppm) and 1 (at 2000 ppm).
4. At 150°C, 100% CO conversion is obtained at an O₂/CO = 1. Selectivity of O₂ for CO is about 50%.

REFERENCES

- (1) G. Acres, J. Frost, G. Hards, R. Potter, T. Ralph, D. Thompson, G. Burstein and G. Hutchins, *Catalysis Today* 38 (1997) 393
- (2) R. Singh, *Chemical Engineering Progress*, 95(3),59 (1999)
- (3) M. Twigg, *Catalyst Handbook*, Wolfe Publishers, London, England, 1989; Chapters 4-7
- (4) M. Brown and A. Green, US 3,088,919 (May 7, 1963)
- (5) J. G. Cohn, US 3,216,782 (November 9, 1965)
- (6) M. Brown, A.S. Green, J.G. Cohn and H. Anderson, *Ind. Eng. Chem.* 52(10)841(1960)

Table 1
Comparison of Powdered Pt/Al₂O₃ and Monosel Catalysts
 (fraction 40-60 μ, VHSV~120,000 hr⁻¹)

#	TEST CONDITIONS	Monosel		Pt/Al ₂ O ₃	
		X _{co} , %	X _{O₂} for CO, %	X _{co} , %	X _{O₂} for CO, %
1.	At 90°C, O ₂ /CO=0.5	51	78	13.2	82
2.	At 90°C, O ₂ /CO=0.75	90	65	12.7	66.2
3.	At 150°C, O ₂ /CO=0.5	52.7*	61.6*	26.8	56.7

*) data were obtained with monosel on a monolith at a VHSV = 80,000 h⁻¹

Table 2
Effect of CO Concentration on Monosel Performance

#	TEST CONDITIONS	2000 ppm CO			5000 ppm CO		
		X _{co} , %	X _{O₂} , %	X _{O₂} for CO %	X _{co} , %	X _{O₂} , %	X _{O₂} for CO %
1	At 90°C, O ₂ /CO = 0.5	68.9	98.1	66.1	69.0	87.0	77.6
2	At 90°C, O ₂ /CO = 0.75	96.8	97.5	64.4	100	99.7	68.1
3	At 90°C, O ₂ /CO = 1.0	100	99.6	50.7	-	-	-
4	At 150°C, O ₂ /CO = 1.0	100	99.7	50.6	100	100	50.9
5	At 150°C, O ₂ /CO = 0.75	90.6	99.5	57.8	97.5	100	64.6
6	At 150°C, O ₂ /CO = 0.5	61.2	99.2	57.7	65.6	99.4	64.6

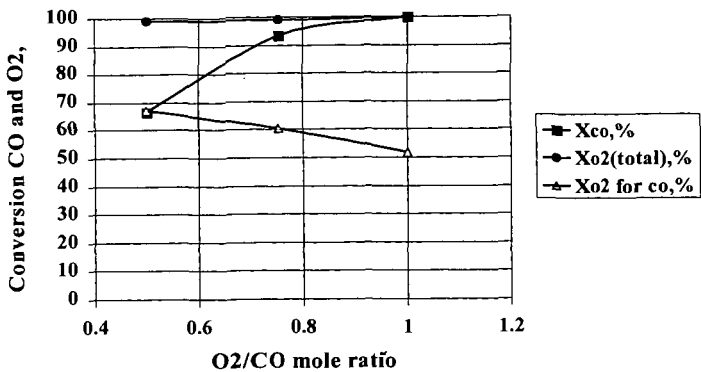


Fig. 1. Monosel on monolith activity and selectivity depends on O₂/CO (90°C, 1,000 ppm CO, 20% H₂, 10% H₂O, VHSV=20,000 hr⁻¹)

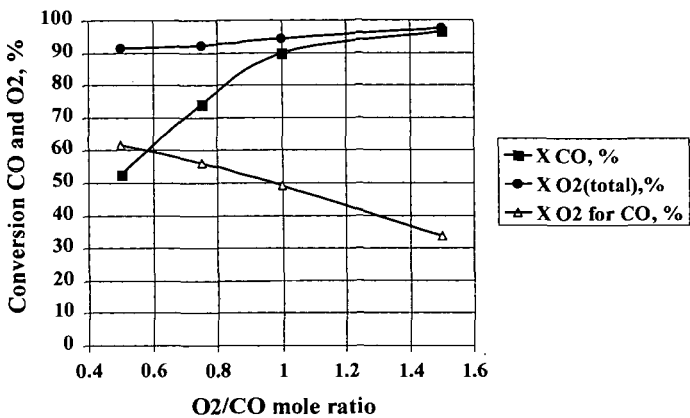


Fig. 2. Monosel on monolith activity and selectivity depends on O₂/CO mole ratio (150°C, 1,000 ppm CO, 20% H₂, 10% H₂O, VHSV=80,000 hr⁻¹)

CATALYTIC REACTOR FOR IMPROVED CARBON MONOXIDE CONTROL WITHIN THE HYDROGEN FEED STREAM OF A PEM FUEL CELL

J. K. Hong, M. A. Inbody, J. C. Hedstrom, J. I. Tafoya and N. E. Vanderborgh

Fuel Cell Engineering
ESA-EPE, Los Alamos National Laboratory
Los Alamos, NM 87545 USA

KEYWORDS: PEM Fuel Cell, Carbon Monoxide Removal, Preferential Oxidation

INTRODUCTION

The proton exchange membrane (PEM) fuel cell is considered a promising energy conversion device, based on environmental and energy efficiency advantages.¹ Even though hydrogen-air PEM fuel cell systems have been considerably improved over the past two decades, direct hydrogen systems present challenges for wide-spread automotive applications.² The advantage of contemporary fuel cells becomes compromised if their deployment requires a new complicated hydrogen infrastructure. On-board reforming of contemporary clean fuels is an alternative approach for supplying hydrogen for these PEM fuel cell vehicles. Fuels for such clean vehicles include natural gas, reformulated gasoline, alcohols, ethers and other hydrocarbons.³ Chemical conversion of these fuels using either partial oxidation or steam reforming generates a hydrogen stream diluted with carbon dioxide, nitrogen, steam and various contaminants including carbon monoxide. In the presence of CO stack efficiency is compromised, so fuel processing hardware must include features to manage impurities. The Fuel Cell Engineering Team at Los Alamos has pioneered successful approaches for gas cleanup. The effort combines catalyst development with novel reactor designs, perhaps suitable for future automotive applications. These large-scale experiments are supported by micro-scale investigations of catalyst performance. One important focus is to develop new approaches useful for achieving transient behavior of contemporary passenger vehicles. Such a gas clean-up device is termed a PROX (preferential oxidation) converter, even though oxidation is but one of the several reactions necessary for successful fuel cell system hardware.⁴

EXPERIMENTAL

Both micro-scale and larger (50-kW) device experiments are described. The micro-scale test stand permits catalyst evaluation using test gas mixtures selected to replicate operation with a variety of fuels, such as might result using a "multifuel reformer". For instance a simulated gasoline reformatte might consist of 36% H₂, 17% CO₂, 28% N₂ and 17% H₂O. Small quantities of contaminants are added to such mixtures and then the mixtures are blended with controlled quantity of air. The resulting mixture is transferred to a volume of catalyst. Analytical tools including gas chromatography and gas chromatography mass spectrometry evaluate catalyst effectiveness. Considerable attention is paid to the fluid dynamics of the experiments to assure uniform gas composition, inlet temperature and laminar flow. These reactors can be either adiabatic ("hot spot") or isothermal, depending upon test conditions. The micro-scale reactor is used to determine performance data on a variety of catalyst types and to investigate techniques for effective control of other contaminants such as NH₃ or H₂S.

The large scale experiments replicate conditions used for microscale testing. One PROX reactor with three series, adiabatic sections is shown in Figure 1. Each section incorporates features to homogenize the gas mixture, to control entrance temperature and to assure laminar flow into the catalyst volume. Heat flow is primarily through convective processes. The overall large-scale design includes features designed to meet safety standards for hydrogen operation and to permit convenient exchange of catalyst samples and alteration of other internal features. The large experiment also permits dynamic measurement of gas composition and temperature within the catalyst volume to measure either "down the channel" or spatial (radial) data. Such information has proven very useful to confirm modeling predictions.

Experiments are computer controlled. The electronic systems sets appropriate reactant flows and controls temperatures and pressure. Importantly the data system also continuously evaluates for experimental faults such as hydrogen leaks and acts to terminate tests when certain release rates are reached.

RESULTS

Preferential oxidation depends upon rapid CO oxidation even in the presence of far larger mole fractions of hydrogen. The intent is to remove the CO with only small concurrent hydrogen oxidation. Although there have been significant improvements in anode fuel cell catalysts to increase CO tolerance, most contemporary systems dictate that inlet CO concentration should be set at below 30 ppm.

The removal rate of CO through oxidation on a platinum catalyst in the micro-scale reactor depends on the reaction temperature, as shown in Figure 2. The highest conversion of CO, or the lowest outlet CO concentration, is attained at 220°C and by further increase in reaction temperature leads to high outlet CO concentration. Additional experimental results support that increased CO found at temperatures exceeding 220°C is attributed to the rapid hydrogen oxidation at these temperatures which depletes oxygen and concurrent production of CO by the reverse shift reaction.

The inlet oxygen concentration was varied as shown in Figure 3 and the effect on CO control was measured. The outlet CO concentration was determined at 220°C and 260°C, respectively. At both reactions temperatures, oxygen is rapidly depleted by reaction with CO and H₂ at oxygen stoichiometry as high as to 3.0 based on the CO concentration. In this case a stoichiometry value of 1.0 is defined, for example, when the number of moles of oxygen is 0.5 that of the moles of CO—for example 250 ppm of oxygen, as a constituent of air, is added to a stream containing 500 ppm of CO. From Figure 3, an increase in oxygen stoichiometry at 220°C is found to be effective in reducing outlet CO concentration, while concurrent hydrogen loss is significant with the increase in oxygen stoichiometry at 260°C.

Figure 4 shows PROX device performance as a function of overall oxygen stoichiometry, summed for each of the stages based on the inlet CO content. Figure 4 shows results for an inlet concentration of 20,000, using three stages. The device output ranges from a CO concentration of 45 ppm to well below 20 ppm, depending upon conditions. In general these hydrogen-mixture cleanup devices perform as designed over a wide range of flow rates and inlet carbon monoxide concentrations.

Transient performance, CO control during a rapid change in either CO concentration or flow rate, can be achieved by either precise control of reactant flows or through intelligent catalyst design, or by a combination of these approaches. Transient performance at the 50-kW flow level during an event when a normal 8,000 ppm CO flow stream is changed to a 12,000 ppm CO gas stream. With appropriate alteration of the air injection rate, the device shows no performance degradation.

Other contaminants than carbon monoxide are troublesome. Some compounds will not influence PROX performance but can degrade stack performance. Others tend to poison the catalyst surfaces contained in the PROX device. The hydrogen generators also, at times, generate colloidal carbon ("soot"), a contaminant that can adversely influence PROX performance.

CONCLUSIONS

Gas cleanup-technology is an essential operation in on-board fuel processing systems. Today transportation fuel specifications are being adjusted to meet increasingly demanding environmental emission regulations. Cleaner fuels, especially low sulfur fuels, are more easily processed as hydrogen sources. New fuels, such as dimethyl ether, dimethoxy methane and gas-to-liquid ("Fischer Tropsch") compounds are additional steps along the pathway towards very clean vehicles. All of these clean fuels are also attractive candidates for fuel cell vehicles.

Although there has been considerable progress in gas clean-up technology, challenges remain. Such devices must address automotive applications with special requirements for low initial cost, ruggedness and reliability. Transients are also challenging, especially the transient during start-up of the vehicle. In these experiments the gases are

added to the catalyst at a temperature exceeding the "light-off" temperature. Special designs will be necessary to initiate operation within the 20 seconds, or so requirement, following a cold-soak period. Even so, much of the necessary technical design challenges for these devices have been successfully demonstrated.

REFERENCES

1. Nicholas E. Vanderborgh and Michael A. Inbody, "The Future of Fuel Cell Vehicles", presented at the 3rd Annual Symposium, Society of Electric Vehicle, Kawasaki, JP, December 2, 1998; LA-UR# 98-5858.
2. Firtz R. Kalhammer, Paul R. Prokopius, Vernon Roan and Gerald E. Voecks, "Status and Prospects of Fuel Cells as Automotive Engines, A Report of the Fuel Cell Technical Advisory Panel", prepared for the States of California Air Resources Board, Sacramento, CA, July 1998.
3. S. Ahmed, M. Krumpelt, R. Kumar, S. H. D. Lee, J. D. Carter, R. Wilkenhoener and C. Marshall, "Catalytic Partial Oxidation Reforming of Hydrocarbon Fuels", presented at Fuel Cell Seminar, Palm Springs, CA, November 1998.
4. Nicholas E. Vanderborgh, James C. Hedstrom, Jose Tafoya and Michael A. Inbody, "Preferential Oxidation for Improved Performance of PEM Fuel Cell Anode Feeds", presented at the Electrochemical Society Meeting, Seattle, Washington, May 4, 1999.

ACKNOWLEDGEMENT

This work is supported by the United States Department of Energy, through its Office of Advanced Automotive Technologies.

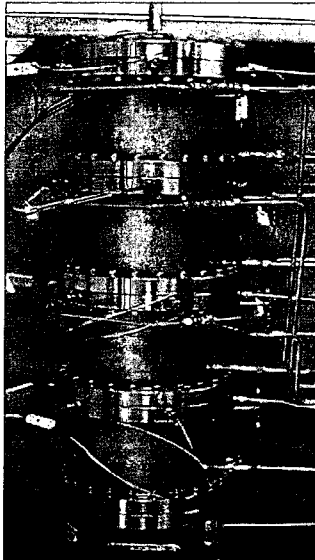


Fig. 1 The 50kW modular PROX assembled at the PROX test facility.

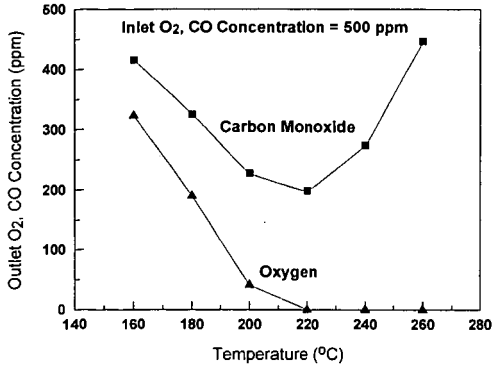


Fig. 2 The measured outlet oxygen and carbon monoxide concentrations with reaction temperature.

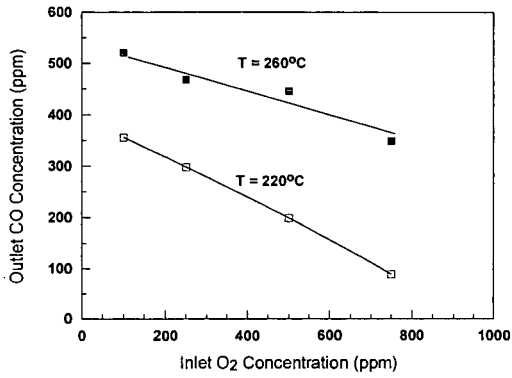


Fig. 3 The measured outlet carbon monoxide concentration as a function of inlet oxygen concentration.

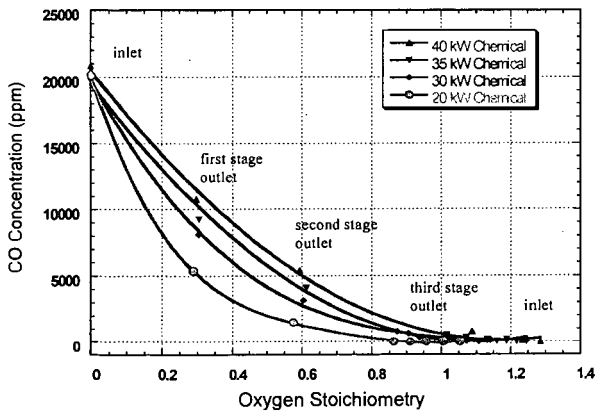


Fig. 4 PROX device performance as a function of overall oxygen stoichiometry.

COMPACT FUEL PROCESSORS FOR FUEL CELL ELECTRIC VEHICLES (FCEVs)

W. L. Mitchell, Prashant S. Chintawar, Mark Hagan, Bo-Xiong He, and S. K. Prabhu
Epyx Corporation, 15 Acorn Park, Cambridge, MA 02140

Keywords: fuel processing, fuel cell electric vehicles, reformer

Introduction

Faced with tough emission standards, auto manufacturers have started looking into technologies that offer feasible alternatives to internal combustion engines. Fuel cells offer many advantages including almost-zero emissions. Epyx Corporation, a subsidiary of Arthur D. Little, Inc., has developed a fuel-processor design that reforms hydrocarbon such as gasoline and generates hydrogen – needed to run fuel cell. In fact, Epyx is the first company ever to demonstrate a gasoline-based reformer. In addition to its lightweight and compact configuration, Epyx fuel processor operates on multiple fuels such as gasoline, ethanol, propane, and natural gas.

Background

Proprietary hybrid partial oxidation (POX) fuel processor is shown in Figure 1. The fuel processor consists of a series of catalytic beds, viz., steam reforming, high temperature shift (HTS), low temperature shift (LTS) and exhaust clean-up, operating over a wide temperature range to maximize hydrogen output. The exit CO concentration from the fuel processor is 0.2-0.5 % depending on the steam/carbon (S/C) ratio and temperature. However, for a proton exchanged membrane (PEM) fuel cell applications, the CO concentration must be below 50 ppm. Therefore, an additional CO clean-up stage called preferential oxidation (PROX) is also included. For the processing of sulfur containing fuels, the fuel processor also contains a compact desulfurization bed integrated inside the reactor vessel.

A fraction of the feedstock is combusted in the POX zone at about 700-1500 °C. The process effluent from POX zone consists of a mixture of CO, CO₂, H₂, H₂O, N₂ and residual methane. A highly active steam reforming bed holds the key to full fuel conversion and high efficiency. The POX residual methane is reformed into hydrogen in the steam reforming bed and CO is converted in the two shift reactors, viz., HTS and LTS.

Experimental

Based on the results from previous work at Epyx/A. D. Little, Inc., a fuel processing power system was designed using assumptions consistent with a light duty vehicle. The fuel processor system consists of three subsystems, viz., fuel processor, CO clean-up, and tailgas combustor. The assumptions involved in the design of the fuel processor include a use of PEM fuel cell operating at 3 atm and at a design power level of 10 kW (electric). The design power rating power corresponded to a fuel processor system that could operate on a thermal input of 45 kW.

Experimental studies were carried out to permit characterization of the entire system with regard to thermal balances, pressure balances, hydrogen purity effects, tailpipe emissions, and required control interaction. The system was operated on several conventional and alternative automotive fuels such as California Phase II reformulated gasoline (RFG), ethanol, natural gas, etc. The performance of fuel processor was quantified by measuring the conversion efficiency at a particular S/C ratio and equivalence ratio (ϕ).

To quantify the emissions from the fuel processor assembly, the exhaust product sample was connected to various analytical instruments listed below:

- Gas chromatograph equipped with a thermal conductivity detector (GC/TCD) for detection and quantification of H₂, N₂, CH₄, C₂H₂, C₂H₄, CO₂, and CO;
- Non-dispersive infra-red (NDIR) analyzer for CO and CO₂;
- Chemiluminescent NO_x analyzer;
- Flame ionization detector (FID) hydrocarbon analyzer;

- Paramagnetic oxygen analyzer.

Results and Discussion

Recent efforts have focussed on incorporating advanced catalyst and heat exchanger concepts into the fuel processor design. This new generation of the design is sized to accommodate a 22 kW (electric) fuel cell power system. Experiments were conducted on this design with a variety of fuels and the fuel processor was characterized in terms of temperature and composition of each zone, operating conditions for the POX zone, and conversion efficiency.

The performance of the fuel processor measured as hydrogen efficiency with all the fuels is shown in Table 1. Hydrogen efficiency is defined on the basis of lower heating value of H₂ exiting the fuel processor to the lower heating value of the fuel fed to the unit. The extended testing of this new design indicate that advanced concepts employed have led to significant improvements in the efficiency, which exceed the 2004 Department of Energy PNGV (Partnership for New Generation of Vehicles) efficiency targets for fuel processors – currently set at 80%. It is also evident from Table 1 that such high efficiency of the fuel processor results in high fuel conversion or low slip of unconverted hydrocarbons, which assist in obtaining very low exhaust emissions. No degradation in the performance of the catalyst beds was evident after 600 h on-stream – a ramification of high fuel conversion.

Table 1. Epyx transportation fuel processor performance with various fuels

Fuel	Dry H ₂ concentration* (%)	Fuel conversion (%)	Efficiency** (%)
RFG	43	98	83
Methanol	46	99	88
Ethanol	42	99	84
Natural gas	45	95	83

*: at the exit of the fuel processor

** : defined as ratio of lower heating value of H₂ at the exit to the lower heating value of the fuel fed to the fuel processor

As a first step in verifying the low emissions produced from a gasoline fed fuel processor, steady state emissions analysis was performed at the exhaust of tailgas combustor. Emission data gathered at 25 kW (thermal) input to the fuel processor show CO < 5 ppm, hydrocarbons < 4 ppm, and undetectable levels of NO_x. Assuming FUD cycle with 12.5 kW (electric) average power requirement yields emissions in g/mile as shown in Table 2.

Table 2. Comparison of Epyx fuel processor emissions with California SULEV standards

Contaminant	California SULEV standard (g/mile)	Epyx fuel processor (g/mile)
CO	1.0	0.013
Hydrocarbon	0.01	0.017
NO _x	0.02	0.003

These emissions are expected to reduce with modifications and tighter integration of the system.

Conclusions

Compact automotive fuel processor was designed, fabricated and tested with gasoline, natural gas, methanol, and ethanol. This design demonstrated efficiency numbers greater than PNGV 2004 targets and emissions comparable with California SULEV standards. Pathways have been identified to further improve the overall performance of the fuel processor. Detailed reaction models are being generated and validated; these models will be used in the future designs.

Acknowledgements

This work was funded by US Department of Energy, Office of the Transportation Technologies and co-funded by Illinois DCAA. Parts of this work were performed in conjunction with Plug Power LLC.

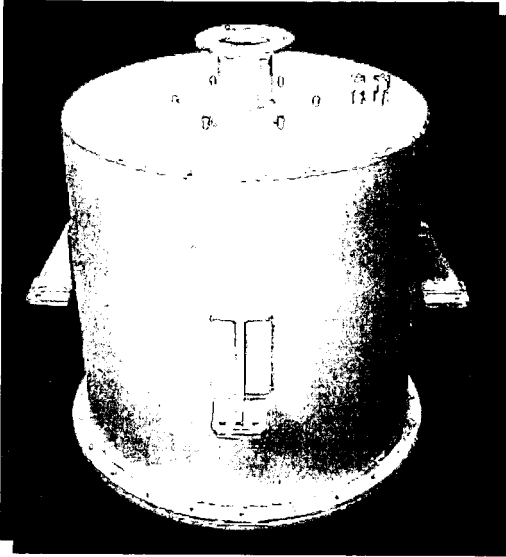


Figure 1. Epyx 22 kW (electric) multi-fuel processor